CONTRAST MEDIA & MOLECULAR IMAGING

Received: 13 November 2012, Revised: 24 July 2013, Accepted: 1 August 2013, Published online in Wiley Online Library

(wileyonlinelibrary.com) DOI: 10.1002/cmmi.1564

Monitoring hypoxia and vasculature during bevacizumab treatment in a murine colorectal cancer model

L. Heijmen[a]*, E. G. W. ter Voert[b], C. J. A. Punt[c], A. Heerschap[b], W. J. G. Oyen[d], J. Bussink[e], C. G. J. Sweep[f], P. Laverman[d], P. N. Span[e], L. F. de Geus-Oei[d], O. C. Boerman[d] and H. W. M. van Laarhoven[a,c]

The purpose of this study was to assess the effect of bevacizumab on vasculature and hypoxia in a colorectal tumor model. Nude mice with subcutaneous LS174T tumors were treated with bevacizumab or saline. To assess tumor properties, separate groups of mice were imaged using ^{18}F-Fluoromisonidazole (FMISO) and ^{18}F-Fluorodeoxyglucose (FDG) positron emission tomography or magnetic resonance imaging before and 2, 6 and 10 days after the start of treatment. Tumors were harvested after imaging to determine hypoxia and vascular density immunohistochemically. The T_2* time increased significantly less in the bevacizumab group. FMISO uptake increased more over time in the control group. Vessel density significantly decreased in the bevacizumab-treated group. The Carbonic anhydrase 9 (CAIX) and glucose uptake transporter 1 (GLUT1) fractions were higher in bevacizumab-treated tumors. However, the hypoxic fraction showed no significant difference. Bevacizumab led to shorter T_2* times and higher GLUT1 and CAIX expression, suggesting an increase in hypoxia and a higher glycolytic rate. This could be a mechanism of resistance to bevacizumab. The increase in hypoxia, however, could not be demonstrated by pimonidazole/FMISO, possibly because distribution of these tracers is hampered by bevacizumab-induced effects on vascular permeability and perfusion.

Keywords: bevacizumab; colorectal cancer; hypoxia; mechanism of resistance; tumor vasculature and microenvironment

1. INTRODUCTION

Bevacizumab (Avastin®) is an antibody against vascular endothelial growth factor (VEGF), inhibiting VEGF stimulated angiogenesis (1). In advanced colorectal cancer, bevacizumab has been shown to increase progression-free survival, when combined with cytotoxic treatment (2–5). The exact mechanism of action of bevacizumab has not yet been clarified, nor are mechanisms of resistance to bevacizumab understood. It has been suggested that bevacizumab leads to vascular normalization of tumor vessels, thereby increasing delivery of cytotoxic agents to the tumor and thus improving treatment efficacy (6,7). In contrast, other hypotheses claim that bevacizumab may lead to the formation of inadequate tumor vessels, inducing tumor hypoxia and necrosis (8). Although inadequate vasculature and tumor hypoxia may subsequently lead to tumor necrosis, induction of hypoxia could also drive progression toward a more aggressive tumor phenotype (9,10). Hypoxic tumors are less responsive to systemic therapy and radiation therapy (11,12). This could explain the suboptimal results of bevacizumab treatment in various cancer types, including breast cancer (13–15). The suboptimal results have recently led to withdrawal of US Food and Drug Administration approval for the use of bevacizumab in combination with paclitaxel in metastatic breast cancer (16).

In this study we aim to assess the biological effects of bevacizumab over time in a colorectal cancer model. Functional imaging techniques were used to assess the biological effects of bevacizumab on hypoxia and functional vasculature, since these *in vivo* measurements provide the opportunity for repeated measurements and can also be implemented in clinical studies.

* *Correspondence to: L. Heijmen, Department of Medical Oncology, Radboud University Nijmegen Medical Centre, Nijmegen, The Netherlands. E-mail: l.heijmen@onco.umcn.nl*

a *L. Heijmen, H. W. M. Laarhoven*
Department of Medical Oncology, Radboud University Nijmegen Medical Centre, Nijmegen, The Netherlands

b *E. G. W. Voert, A. Heerschap*
Department of Radiology, Radboud University Nijmegen Medical Centre, Nijmegen, The Netherlands

c *C. J. A. Punt, H. W. M. Laarhoven*
Department of Medical Oncology, Academic Medical Center, University of Amsterdam, Amsterdam, The Netherlands

d *W. J. G. Oyen, P. Laverman, L. F. Geus-Oei, O. C. Boerman*
Department of Nuclear Medicine, Radboud University Nijmegen Medical Centre, Nijmegen, The Netherlands

e *J. Bussink, P. N. Span*
Department of Radiation Oncology, Radboud University Nijmegen Medical Centre, Nijmegen, The Netherlands

f *C. G. J. Sweep*
Department of Laboratory Medicine, Radboud University Nijmegen Medical Centre, Nijmegen, The Netherlands

^{18}F-Fluoromisonidazole (FMISO) is a nitro-imidazole derivative, which is reduced into intermediary metabolites by intracellular enzymes at low intracellular pO_2. After bioreduction, FMISO (metabolites) are trapped in hypoxic cells, allowing for positron emission tomography (PET) imaging of hypoxic tumors (17). Thus, FMISO PET is sensitive to hypoxia and, therefore, could provide an answer to whether treatment with bevacizumab increases tumor hypoxia. However, no FMISO PET data after bevacizumab treatment are available.

^{18}F-Fluorodeoxyglucose (FDG) PET is sensitive to changes in tumor glucose metabolism over time. FDG uptake depends on expression of GLUT1, the main glucose and FDG transporter, and the presence and activity of the enzyme hexokinase. FDG uptake is also dependent on tumor vascularity for supply of FDG and might be influenced by tumor hypoxia owing to the Pasteur effect (18,19). However, tumors often exhibit enhanced glycolysis under normoxic conditions (Warburg effect) for ATP production. FDG PET has been shown to have predictive value for response to several cytostatic treatments (20), including bevacizumab-containing treatments (21–23).

In contrast to FDG PET, dynamic contrast enhanced magnetic resonance imaging (DCE-MRI) is a direct measurement of functional vasculature. Various DCE-MRI parameters, such as the area under the contrast–concentration curve (AUC), blood volume, K^{trans} and k_{ep} have been shown to change after administration of antiangiogenic or antivascular drugs (21,24,25). Similarly, T_2* MRI can be used to assess vascular properties, without the requirement for the administration of contrast agents. T_2* MR contrast arises from local inhomogeneities of the magnetic field mainly owing to the tissue level of blood deoxyhemoglobin (26). Therefore, T_2* measurements are dependent on hypoxia, blood flow and blood volume (27).

In this study, we assessed the effect of bevacizumab on functional imaging parameters with FMISO PET, FDG PET, DCE-MRI and T_2* at different time points after start of treatment, to assess whether bevacizumab increases hypoxia owing to a disruption of tumor vasculature. Immunohistochemical analyses were used to corroborate our results.

2. MATERIALS AND METHODS

2.1. Animals

Seventy female BALB/c nu/nu mice of 19-24 grams and 6–8 weeks of age were purchased from Janvier (Uden, the Netherlands). Mice were allowed to adapt for one week after transport and were held in a controlled environment in accordance with institutional guidelines (temperature 22 °C, humidity 61%, 12 h light–dark cycle, in individually ventilated cages). Food and water were supplied *ad libitum*.

Mice were injected subcutaneously, just above the rights scapula, with ~1×10^6 cells of the bevacizumab-sensitive human colon cancer cell line LS174T (CCL-188; passage 7; American Type Culture Collection, Manassas, VA, USA). After 14 days, tumors had grown to a maximum diameter of 0.4–0.8 cm and treatment was started. Animals were divided into four groups: two experimental groups undergoing MR and PET imaging, respectively; and two control groups undergoing MR and PET imaging. For each day of imaging, a separate group of mice was used, except for the sequential PET imaging days. In order to reduce the burden of repetitive anesthesia for each mouse, to make sure overall drop out was low and measurements were reliable, separate groups of five mice were used for PET and MR imaging on each day (Fig. 1). All experiments were approved by the Animal Welfare Committee of the Radboud University Medical Centre.

2.2. Treatment

In the experimental group, bevacizumab (Avastin®, Roche Pharma, Germany) was administered twice a week (during 10 days) by intraperitoneal injection in a dose of 5 mg/kg. The control group received an intraperitoneal injection with 0.9% saline at the same time points.

2.3. Imaging

PET imaging was performed on an preclinical PET scanner (Inveon, Siemens USA Inc., Knoxville, TN, USA). FMISO PET imaging was performed before treatment and 1, 5 and 9 days after the start of bevacizumab therapy. FDG PET imaging was performed before treatment and 2, 6 and 10 days after the start of bevacizumab therapy (Fig. 1). Before FDG PET imaging, mice fasted for 12 h. Ten min before administration of FDG, mice were anesthetized with isoflurane 4% for induction and 1.5-2% for maintenance. A 60 min interval between injection of FDG and FMISO and the start of the PET scan was used. All PET scans were performed using 20 min single-bed position measurements. Mice were injected intravenously in an inserted tail vein cannula with a solution of approximately 10 MBq of the radiotracer in 0.2 ml 0.9% saline. Images were reconstructed using OSEM-3D-MAP reconstruction. The highest standardized uptake values (SUV_{max}) for both FMISO and FDG PET were recorded for each tumor, by drawing a region of interest around the entire tumor. In general, SUV_{max} demonstrates a larger change after start of treatment than SUV_{mean}. Therefore, the SUV_{max} values are reported.

MR imaging was performed on a 7 T small animal MR scanner (Clinscan, Bruker Biospin, Ettlingen, Germany) using a Bruker rat brain receiver coil. Imaging was performed at baseline and 2, 6 and 10 days after start of therapy.

DCE-MRI was performed using a T_1 weighted fast low-angle shot sequence. Sequence parameters were as follows: repetition time (*TR*) 90 ms, echo time 1.82 ms, flip angle 15°, 16 slices with a thickness of 1 mm, field of view 30 mm, matrix size 64 × 64.

After approximately 6 s, 0.2 ml (0.02 mmol/ml) of the contrast agent Gadomer-17 (Schering AG, Berlin, Germany) was injected in the tail vein cannula.. Before and after DCE-MRI, proton density images were recorded with the same sequence parameters as the DCE-MRI except for the flip angle of 20° and *TR* 1500 ms. Data from these images were combined with the DCE-MRI data to calculate the concentration of Gadomer-17, using the method described by Hittmair *et al.* (28). Area under the concentration peak was calculated for 0–90 and 0–180 s after contrast injection.

T_2* imaging was performed with a gradient echo sequence, with a *TR* of 1000 ms and six different echo times (*TE*): 2.78, 4.86, 6.89, 8.92, 10.95 and 12.98 ms. Eighteen 1 mm slices were obtained with two averages. T_2* calculated maps were generated using in-house built software based on Matlab (MathWorks, Natick, MA, USA). The data were fitted pixel-by-pixel to a mono-exponential curve $SI = A\rho\exp(-TE/T_2^*) + B$ where ρ is the proton density, *TE* is the echo time, and the parameter of interest T_2*, the relaxation time. The regions of interest for the MR images were manually drawn on T_2 images and copied onto the T_2* map and contrast concentration images.

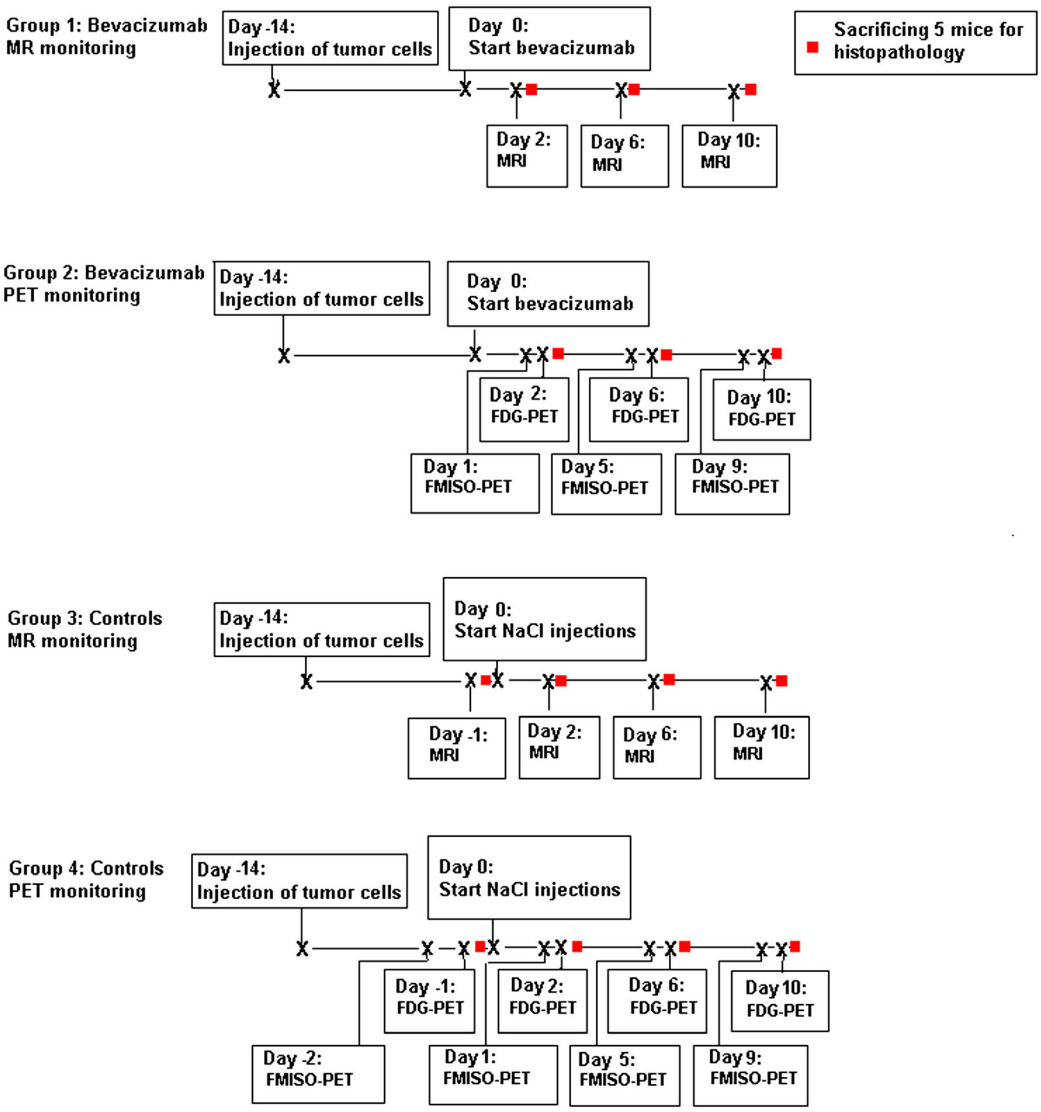

Figure 1. Schedule of imaging and sacrifice of the mice.

2.4. Immunohistochemistry

To correlate *in vivo* hypoxia and vasculature measurements with *ex vivo* measurements, all mice were euthanized immediately after the last scan. Respectively 50–80 and 2 min before death, the hypoxic marker pimonidazole {80 mg/kg in 0.1 ml; 1-[(2-hydroxy-3-piperidinyl) propyl]-2-nitroimidazole hydrochloride; Natural Pharmacia International, Research Triangle Park, NC, USA} and the perfusion marker Hoechst 33342 (Sigma Chemical Co., St Louis, MO, USA) were administered. Tumors were removed and snap-frozen in liquid nitrogen. They were stored at −80 °C.

Tumor sections (4 μm) were fixed in acetone at 4 °C for 10 min and washed with phosphate buffered saline (PBS). The sections were incubated overnight at 4 °C with a rabbit anti-pimonidazole (gift from J. A. Raleigh, Department of Radiation Oncology, University of North Carolina School of Medicine, Chapel Hill, NC, USA) in primary antibody diluent (1:1000; PAD, Abcam, Cambridge, UK). Sections were rinsed three times with PBS. To stain the vasculature, undiluted 9F1 (rat anti-mouse endothelium, Department of Pathology, Radboud University Medical Center) was applied to the slides for 45 min at 37 °C.

To extend our data concerning hypoxia and functionality of the vessels after bevacizumab treatment, all tumors harvested on day 10 were stained for CAIX and glucose uptake transporter 1 (GLUT1). Sections were pre-incubated for 30 min in 5% normal donkey serum in PAD. CAIX was stained by applying rabbit anti-CAIX-biotin (Novus Biologicals NB100-417B; 1:500 in PAD) overnight at 4 °C followed by mouse anti-biotin-Alexa4888 (1:200 in PAD) for 30 min at 37 °C. GLUT1 was stained using rabbit anti-GLUT1 (Neomarkers; 1:100 in PAD) overnight at 4 °C and goat anti-rabbit-Cy3 (1:600 in PBS) for 30 min at 37 °C. In between, sections were rinsed three times with PBS. Sections were mounted in Fluorostab.

Using a fluorescence microscope (Axioskop, Zeiss, Göttingen, Germany), all stained sections were digitalized using a computer-controlled motorized stepping stage system. By means of Image Processing Laboratory software (Scanalytics Inc., Fairfax, VA, USA), the tumor area was drawn, excluding necrotic areas. The fraction of positive staining in the total tumor area was calculated, providing the hypoxic fraction (fraction of pimonidazole positive staining) and vascular density (number of vessels within 1 mm^2) (29).

2.5. ELISA procedure for bevacizumab

Bevacizumab concentration in plasma was measured with a one-site enzyme-linked immunosorbent assay (ELISA). In short, 96-well plates (Greiner Bio-One, Alphen a/d Rijn, the Netherlands) were coated overnight at 4 °C with 100 µl VEGF (0.50 µg/ml, Genentech Inc, San Francisco, CA, USA), washed (96PW plate washer, Tecan Group Ltd, Männedorf, Switzerland), and then blocked with 150 µl Superblock (Pierce, Rockford, IL, USA) for 30 min at ambient temperature, washed and further blocked with 300 µl bovine serum albumin (Sigma Chemical, St Louis, MO, USA) for 4 h at ambient temperature. Subsequently, the plate was washed and standards (range 0–10 ng/ml Avastin, Roche, Basel, Switzerland), study samples and a reference sample were placed into the wells; the plate was incubated overnight at 4 °C. After washing, the plate was incubated with 100 µl Mouse anti-Human IgG (Fc) peroxidase (dilution 1:25,000, SouthernBiotech, Birmingham, UK) for 2 h at ambient temperature, again washed and incubated with 100 µl ready-to-use tetramethyl benzidine solution (Kem-En-Tec, Taastrup, Denmark) for 15–20 min for color development. The reaction was terminated by addition of 0.5 M H_2SO_4 and optical density was measured at 450 nm in a Multiskan Ascent plate reader (Lab Systems, Oy, Helsinki, Finland). The analytical sensitivity, defined as the minimum bevacizumab concentration evoking a response significantly different from that of the zero calibrator, was 16 pg/ml. Plasma samples, diluted 4000–24 000 fold, exhibited excellent linearity. Known quantities of bevacizumab were added to six plasma samples. The recoveries in the plasma samples ranged from 87 to 110% with a mean recovery of 98%. In each run the reference preparation, prepared from a pool of plasma from animals treated with bevacizumab, was used to monitor the long-term performance of the assay. The concentration in the reference preparation was 1670 ng/ml, the within-run coefficient of variation (CV) and the between-run CV were 7.0 and 10.0%, respectively.

2.6. Statistical analyses

To compare the course of changes in the parameters over time between the bevacizumab and control group, linear regression analysis was used. Linear regression analysis assessed the effect of treatment over time on hypoxia and vasculature. We assessed the interception of the lines of the bevacizumab and control groups at day 0. When the lines did not intercept at day 0, we started linear regression analyses from day 1 (start of treatment). This method of analysis was used to accommodate a flare-up in (PET) parameters directly after start of treatment. This flare-up directly after start of treatment has been described by Findlay *et al.* (30). If the lines did intercept, the regression analyses were started at the baseline measurements. The difference in the course of the measurement parameters over time in the bevacizumab and control group was expressed in a standard coefficient β. Linear regression analysis was also used to assess whether parameters changed in time independent of treatment. A Student *t*-test was used to test for differences between control and treatment groups at the last time point, since the differences were expected to be largest at the last measurement. Furthermore, a Student *t*-test was used to compare CAIX and GLUT1 staining at the same time point. A Pearson correlation was used to assess correlations between image parameters and histopathology results. *p*-Values 0.05 were considered to be statistically significant. All data were analyzed using SPSS 16.0 (SPSS inc, Chicago, IL, USA).

3. RESULTS

3.1. Tumors

In 69 of the 70 mice, subcutaneous tumor growth was observed. Therefore, 34 mice were imaged with FMISO and FDG PET and 35 mice with MRI, leaving only four mice in the intervention group at day 9 and 10, measured with PET. All other groups contained five mice. Tumor volume (measured with MR) increased over time ($r = 0.46$, $p < 0.01$). The average tumor volume before the start of treatment was 310 ± 156 mm^3, while the average volume 10 days after the start of treatment was 420 ± 137 mm^3 for the intervention group and 783 ± 179 mm^3 for the control group. The increase in tumor volume was significantly larger in the untreated control group compared with the bevacizumab group (standardized coefficient β −0.62, $p = 0.01$; Fig. 2).

3.2. Imaging

FMISO particularly accumulated in the center of the tumor, while FDG uptake was mainly observed at the tumor rim (Fig. 3). FMISO uptake in the tumor as measured by SUV_{max} steadily increased over time from 0.67 g/cm^3 before treatment to 1.43 g/cm^3 at day 9 in the control group. In the bevacizumab group, the SUV_{max} increased from 0.67 g/cm^3 before treatment to 1.25 g/cm^3 at day 1, but thereafter decreased to 0.91 and 0.88 g/cm^3 at days 5 and 9, respectively (Fig. 4A). Regression analysis beginning at the start of treatment showed a significant difference in the course of FMISO uptake between the treated group and the control group, with less hypoxia in the treated group (standardized coefficient β −0.85, $p = 0.04$). At day 10, there was a trend toward a difference between the bevacizumab-treated and control group (0.88 vs 1.43 g/cm^3, $p = 0.07$).

In the control group, the average SUV_{max} of FDG increased from 0.53 g/cm^3 before treatment to 1.08 g/cm^3 at day 2 and then remained stable. In contrast, in the bevacizumab-treated group SUV_{max} of FDG increased on day 2 (1.22 g/cm^3), but decreased again at day 6 and at day 10 (day 6, 1.04 g/cm^3; day 10, 0.88 g/cm^3; Fig. 4B). With linear regression analysis, no significant difference was observed in the course of FDG

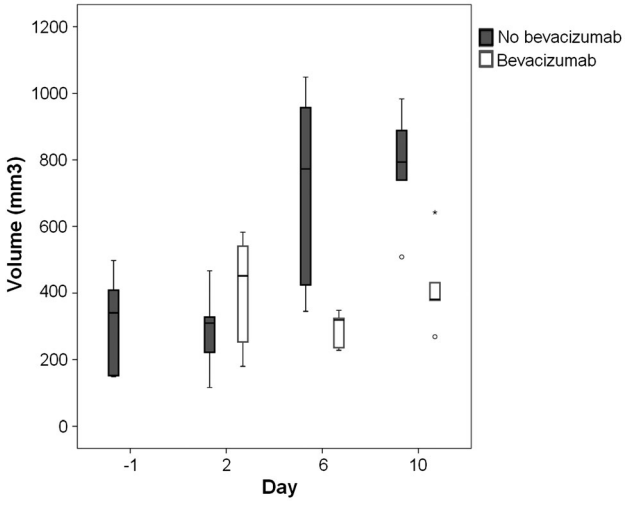

Figure 2. Box plot of the mean tumor volume. The increase in tumor volume was significantly less pronounced in the bevacizumab group (β −0.62, $p < 0.01$).

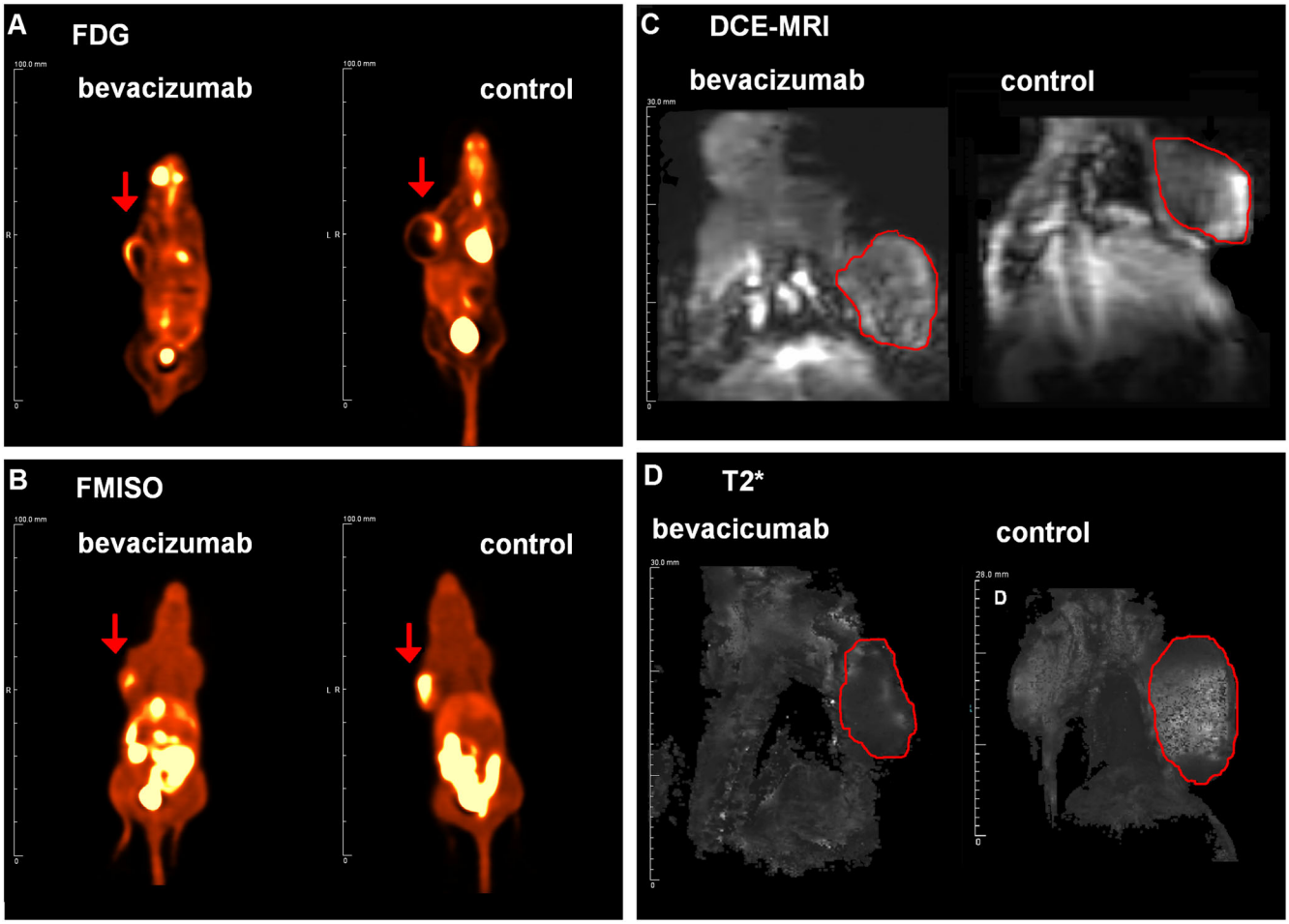

Figure 3. (A) Examples of FDG PET scans showing a treated and untreated tumor, both with high uptake in the rim. The heart and bladder also showed a high FDG uptake. (B) FMISO PET scans showing high FMISO uptake in the center of the tumors, but also high uptake in the intestine and bladder. (C) Dynamic contrast enhanced images and (D) a T_2* maps of a treated and untreated mouse. The tumor borders are marked with a red line.

uptake between the two groups. However, after 10 days the FDG uptake was significantly lower in the bevacizumab-treated group (average SUV_{max} 0.88 vs 1.10 g/cm^3, $p = 0.05$). A positive correlation between FDG PET SUV_{max} and FMISO PET SUV_{max} values was observed ($r = 0.52$, $p = <0.01$).

On DCE-MRI, the AUC_{90} and the AUC_{180} decreased over time in both the bevacizumab-treated and the control group. No significant differences were observed between the two groups, either over time (linear regression analysis) or at the last measurement (Student's *t*-test; Fig. 4C). However, the area under the contrast–concentration curve was significantly lower in larger tumors (for AUC_{180}, $r = -0.45$, $p = 0.02$; for AUC_{90}, $r = -0.44$, $p = 0.02$).

The T_2* value of the tumors increased over time from an average of 3.9 ms before treatment to 7.0 ms on day 10. The rise was more prominent in the control group than in the bevacizumab group (standardized coefficient -0.45, $p = 0.01$). However, there was a large spread in the measurements (Fig. 4D). After 10 days, a trend for a lower average T_2* value was observed in the bevacizumab-treated mice compared with the control group (T_2* at day 10: 5.14 vs 8.94 ms; $p = 0.09$).. The T_2* value correlated to the size of the tumor ($r = 0.68$, $p < 0.01$) in both the treated and untreated tumors.

3.3. Immunohistochemical assessment of tumor hypoxia and vascular density

A typical image of the hypoxia, perfusion and vessels in the colorectal tumor is shown in Fig. 5. The hypoxic areas were well perfused with Hoechst (blue) and high vascular density (red), but areas are overlapping, indicating regions with acute hypoxia: perfused, Hoechst-positive areas that are hypoxic (pimonidazol positive, green). The average hypoxic fraction in the LS174T tumors was 0.38 and did not significantly change over time. Furthermore, no difference in hypoxic fraction was observed between the treated and the control group.

In contrast, CAIX and GLUT1, metabolic markers that are associated with hypoxia, were significantly higher in bevacizumab-treated tumors 10 days after start of treatment (0.22 vs 0.09, p 0.01 and 0.10 vs 0.05, $p = 0.05$; Fig. 6). Before the start of treatment, the average vascular density was 100.7 vessels/mm^2. Vascular density significantly decreased over time in the bevacizumab-treated group compared with the control group (β -0.25, $p = 0.05$). After 10 days of treatment, the vascular density was 74.5 ± 25.4 vessels/mm^2 in the bevacizumab-treated group and 110 ± 36.0 vessels/mm^2 in the control group. There was a significant negative correlation between vascular density

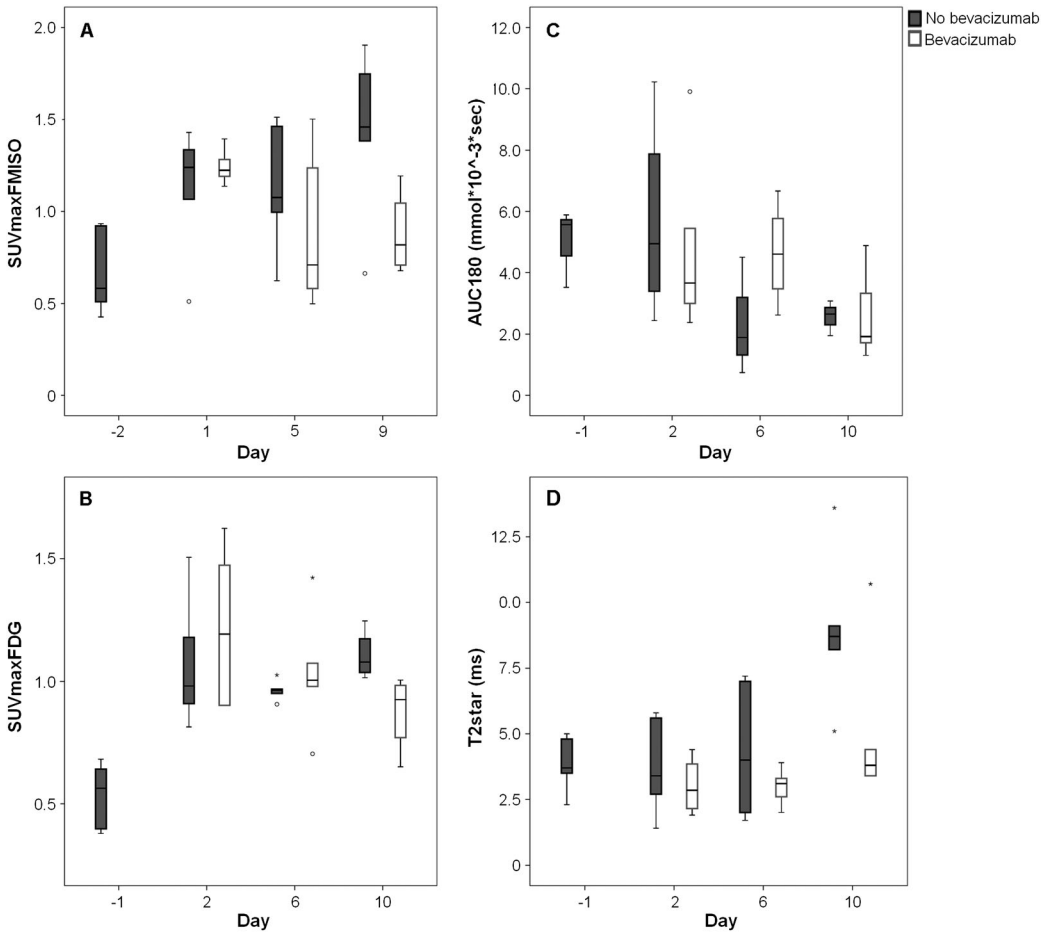

Figure 4. (A) Maximum uptake values of FMISO (*y*-axis) vs the day of treatment (*x*-axis). (B) Maximum uptake values of FDG (*y*-axis) vs the day of treatment (*x*-axis). Maximum FDG uptake at day 10 was significantly lower in the bevacizumab group (white bars) than in the control group (grey bars; $p = 0.01$). (C) AUC_{180} values (*y*-axis) vs the day of treatment (*x*-axis). The AUC_{180} values decreased over time in both treatment and control group. (D) Boxplot of the mean T_2* values (*y*-axis) vs the day of treatment (*x*-axis). The T_2* values increased over time. The rise was more pronounced in the control group (-0.45, $p = 0.01$).

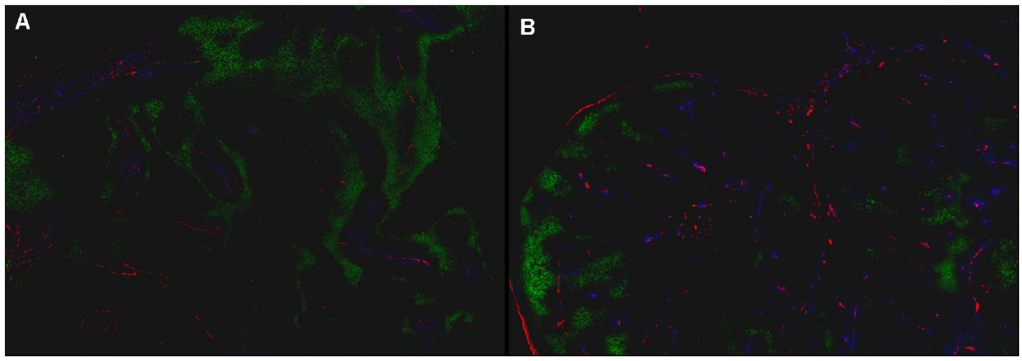

Figure 5. Example of a vital non-necrotic area of (A) an untreated and (B) a bevacizumab-treated tumor 10 days after start of treatment showing the combined image of hypoxia (pimonidazole, green), perfused vessels (Hoechst, blue) and vessels (9F1, red).

and CAIX expression ($r = -0.56$, $p = 0.02$) and a significant positive correlation between CAIX and GLUT1 expression ($r = 0.57$, $p = 0.01$).

Vascular density was positively correlated to AUC_{180} ($r = 0.41$ $p = 0.03$). The average perfused fraction in the tumors was 0.41 and this parameter was unaffected by time or treatment. The perfused fraction did not significantly correlate with vascular density.

3.4. Bevacizumab plasma levels

No bevacizumab was detectable in the control group.. Plasma bevacizumab concentrations increased in the treatment group from an average of 30.2 ± 15.0 μg/ml on day 2 to 56.4 ± 2.3 μg/ml on day 6 and 61.5 ± 16.6 μg/ml on day 10. Bevacizumab concentrations were inversely correlated with

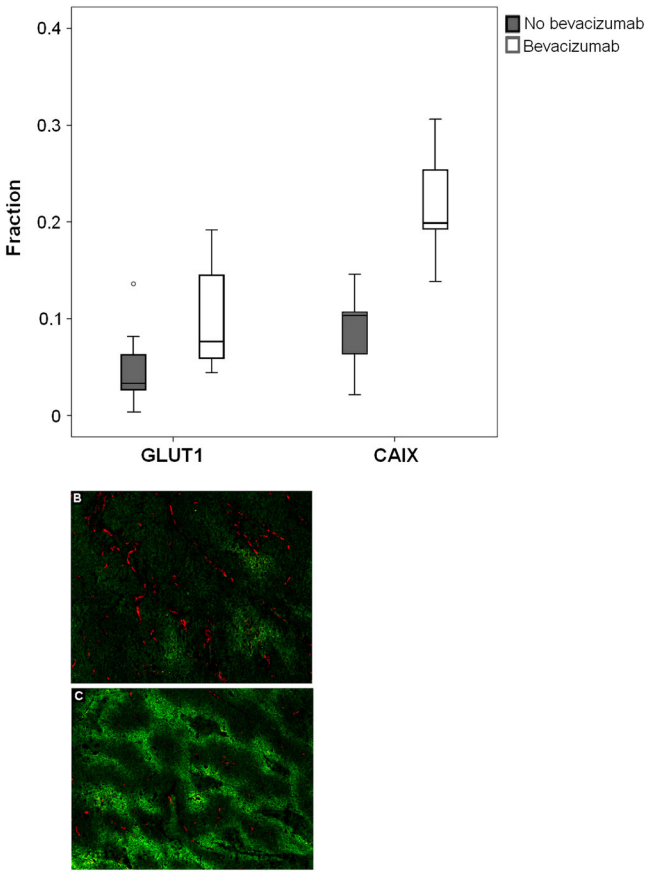

Figure 6. (A) Mean GLUT1 and CAIX staining in the control group and bevacizumab group at day 10. The difference in GLUT1 and CAIX expression differed significantly. (B) An example of an untreated tumor in the control group with low CAIX expression (green) and a high vascular density (red) and (C) an example of a treated tumor in the bevacizumab group of a tumor with a high CAIX expression and a low vascular density.

the immunohistochemically determined vascular density ($r = -0.45$, $p = 0.01$) and positively correlated with CAIX expression in the tumor ($r = 0.77$, $p = 0.02$). Bevacizumab levels did not correlate to imaging parameters.

4. DISCUSSION

In this study, functional imaging techniques were used to assess tumor hypoxia and vascularity after bevacizumab treatment. The FMISO PET imaging technique indicating hypoxia did not show an increase in hypoxia after bevacizumab treatment. In fact, FMISO PET even showed a trend toward a lower FMISO uptake in bevacizumab treated tumors, suggesting a decrease in hypoxia. However, the lower T_2* values measured with MRI in the bevacizumab-treated group pointed toward a higher deoxyhemoglobin concentration and thus hypoxia or a lower blood volume. Also, although pimonidazole binding in bevacizumab-treated tumors did not increase significantly, we observed a marked increase in the hypoxia-related metabolic parameters CAIX and GLUT1 in bevacizumab-treated tumors. Furthermore, the level of bevacizumab in the blood of the mice was inversely correlated to CAIX expression, suggesting a stronger effect with longer and higher dose exposition. Finally, we observed an inverse correlation between CAIX and vascular density. Thus, these data suggest that bevacizumab treatment increases hypoxia in the tumor, which, however, could not be detected by FMISO PET or pimonidazole staining.

There remains the question of how the conflict of data should be interpreted. It is relevant to note that all the techniques that used injected tracers to measure tumor hypoxia failed to show an increase in tumor hypoxia after bevacizumab treatment, while techniques based on intrinsic tumor properties did show an increase in hypoxia. It could be hypothesized that tracer distribution in the tumor is affected by the effect of bevacizumab on the number of functional vessels and vascular permeability. Previously, anti-VEGF has been shown to diminish accumulation of several macromolecules (trastuzumab, anti-EGFR and anti-IGF-1R antibodies) and of chemotherapy (31–33). Moreover, the combination of chemotherapy, cetuximab and bevacizumab led to detrimental outcome in colorectal cancer patients (34), which in part might be due to this phenomenon. The effect of bevacizumab on tumor accumulation of small molecules, such as FMISO, FDG and pimonidazole, is unknown. However, our data also suggest that the uptake of small molecules may be hampered by bevacizumab treatment. Therefore, the interval of 60 min for FMISO scanning may have been too short to reliably detect hypoxia. FMISO imaging in patients generally requires a 2–3 h is generally faster than in humans, and shorter intervals have been described (36), our FMISO results may reflect not only tumor hypoxia, but also tumor vascular supply. In our study, higher blood levels of bevacizumab were associated with lower tumor vascular density. Similarly, in a study monitoring the vascular effects of the vascular disrupting agent (5,6-dimethylxanthenone-4-acetic acid), a marked decrease in FMISO uptake was observed in several tumors, together with a decreased perfusion (36).

In the literature contradictory results have been reported concerning the effect of bevacizumab on tumor hypoxia. In various studies it has been reported that bevacizumab treatment resulted in vascular normalization. In two studies in murine melanoma and glioma models, treatment with bevacizumab decreased the hypoxic fraction measured with pimonidazole, and increased radiosensitivity (37,38). A study in patients with hepatic liver metastases of colorectal cancer who were treated with neoadjuvant chemotherapy and bevacizumab also showed that bevacizumab treatment resulted in tumor vessel stabilization, leading to more mature, stable vessels with an increased diameter, while decreasing the vascular density and increasing necrosis (39). In contrast, several studies showed an increase in pimonidazole positive areas after bevacizumab treatment (40–42). In the literature, hypoxic areas indicated by pimonidazole and CAIX seem to increase after bevacizumab administration, although pimonidazole staining yielded some conflicting results (35–40). The conflicting results using pimonidazole staining support the hypothesis that intravascular tracers might be less reliable after administration of bevacizumab, suggesting that delivery of the tracer might be affected. Pimonidazole does not increase, while hypoxia indeed increases owing to bevacizumab treatment.

However, we did not observe a drop in the perfusion marker Hoechst in the bevacizumab treated group. In line with this interpretation, DCE-MRI parameters AUC_{90} and AUC_{180} were not significantly different between the treated and untreated groups, despite the observed decrease in vascular density in the immunohistochemical analysis of the bevacizumab-treated tumors. These data are in contrast to the theory that bevacizumab significantly hampered the vascular supply of systemically administered tracers.

Alternative explanations for the conflicting results between HIF-1 upregulated markers GLUT1 and CAIX, and pimonidazole and FMISO, are the different pO_2 levels at which CAIX is up-regulated and nitroimidazoles are reduced. CAIX and GLUT1 up-regulation probably starts at a higher pO_2 level than that at which nitromidazoles are reduced (43). Therefore, a small reduction in pO_2 levels caused by bevacizumab treatment might increase CAIX expression without affecting pimonidazole and FMISO uptake. Furthermore, bevacizumab might cause tumor cells to switch toward a more glycolytic, anaerobic metabolism, decreasing the aerobe metabolism and need for oxygen. This implies that these cells could have a high expression of GLUT-1 and CAIX, in order to allow for the high influx of glucose and efflux of the H^+ ions needed for glycolysis, without an increase in hypoxia. Enhanced expression of the endogenous hypoxia marker CAIX was observed after bevacizumab administration in previous studies, and is believed to be a mechanism of resistance to bevacizumab treatment (44). Two studies showed that bevacizumab efficacy increased by inhibiting CAIX or the HIF-1 pathway (41,45).

In conclusion, in this study, bevacizumab treatment induced shorter T_2* times on MR imaging, a higher fraction of the intrinsic hypoxia markers GLUT1 and CAIX on immunohistochemical staining, and a decreased vascular density, suggesting an increase in tumor hypoxia -and glycolysis- mediated by a decrease in tumor vascularity. This could be a mechanism of resistance to bevacizumab. The increase in hypoxia, however, could not be demonstrated by pimonidazole or FMISO, possibly because the distribution of these tracers is hampered by the effects of bevacizumab on vascular permeability and perfusion.

Acknowledgement

This work was supported by a grant from the Dutch Cancer Society (KWF Kankerbestrijding), no. KUN 2008-4098.

REFERENCES

1. Hicklin DJ, Ellis LM. Role of the vascular endothelial growth factor pathway in tumor growth and angiogenesis. J Clin Oncol 2005; 23(5): 1011–1027.
2. Hurwitz H, Fehrenbacher L, Novotny W, Cartwright T, Hainsworth J, Heim W, Berlin J, Baron A, Griffing S, Holmgren E, Ferrara N, Fyfe G, Rogers B, Ross R, Kabbinavar F. Bevacizumab plus irinotecan, fluorouracil, and leucovorin for metastatic colorectal cancer. New Engl J Med 2004; 350(23): 2335–2342.
3. Kabbinavar FF, Schulz J, McCleod M, Patel T, Hamm JT, Hecht JR, Mass R, Perrou B, Nelson B, Novotny WF. Addition of bevacizumab to bolus fluorouracil and leucovorin in first-line metastatic colorectal cancer: results of a randomized phase II trial. J Clin Oncol 2005; 23(16): 3697–3705.
4. Saltz LB, Clarke S, Diaz-Rubio E, Scheithauer W, Figer A, Wong R, Koski S, Lichinitser M, Yang TS, Rivera F, Couture F, Sirzen F, Cassidy J. Bevacizumab in combination with oxaliplatin-based chemotherapy as first-line therapy in metastatic colorectal cancer: a randomized phase III study. J Clin Oncol 2008; 26(12): 2013–2019.
5. Tebbutt NC, Wilson K, Gebski VJ, Cummins MM, Zannino D, van Hazel GA, Robinson B, Broad A, Ganju V, Ackland SP, Forgeson G, Cunningham D, Saunders MP, Stockler MR, Chua Y, Zalcberg JR, Simes RJ, Price TJ. Capecitabine, bevacizumab, and mitomycin in first-line treatment of metastatic colorectal cancer: results of the Australasian Gastrointestinal Trials Group Randomized Phase III MAX Study. J Clin Oncol 2010; 28(19): 3191–3198.
6. Jain RK. Normalization of tumor vasculature: an emerging concept in antiangiogenic therapy. Science 2005; 307(5706): 58–62.
7. Ma J, Waxman DJ. Combination of antiangiogenesis with chemotherapy for more effective cancer treatment. Mol Cancer Ther 2008; 7(12): 3670–3684.
8. Leite de Or, Hamm A, Mazzone M. Growing tumor vessels: more than one way to skin a cat – implications for angiogenesis targeted cancer therapies. Mol Asp Med 2011; 32(2): 71–87.
9. Conley SJ, Gheordunescu E, Kakarala P, Newman B, Korkaya H, Heath AN, Clouthier SG, Wicha MS. Antiangiogenic agents increase breast cancer stem cells via the generation of tumor hypoxia. Proc Natl Acad Sci U S A 2012; 109(8): 2784–2789.
10. Yuan X, Qin L, Xiao-Yu L, Qiu-Ya Y, Wei-Wei X, Gao-Lin L. Short-term anti-vascular endothelial growth factor treatment elicits vasculogenic mimicry formation of tumors to accelerate metastasis. J Exp Clin Cancer Res 2012; 31(1): 16.
11. Brown JM, Wilson WR. Exploiting tumour hypoxia in cancer treatment. Nat Rev Cancer 2004; 4(6): 437–447.
12. Tredan O, Galmarini CM, Patel K, Tannock IF. Drug resistance and the solid tumor microenvironment. J Natl Cancer Inst 2007; 99(19): 1441–1454.
13. Kindler HL, Niedzwiecki D, Hollis D, Sutherland S, Schrag D, Hurwitz H, Innocenti F, Mulcahy MF, O'Reilly E, Wozniak TF, Picus J, Bhargava P, Mayer RJ, Schilsky RL, Goldberg RM. Gemcitabine plus bevacizumab compared with gemcitabine plus placebo in patients with advanced pancreatic cancer: phase III trial of the Cancer and Leukemia Group B (CALGB 80303). J Clin Oncol 2010; 28(22): 3617–3622.
14. Ohtsu A, Shah MA, Van Cutsem E, Rha SY, Sawaki A, Park SR, Lim HY, Yamada Y, Wu J, Langer B, Starnawski M, Kang YK. Bevacizumab in combination with chemotherapy as first-line therapy in advanced gastric cancer: a randomized, double-blind, placebo-controlled phase III study. J Clin Oncol 2011; 29(30): 3968–3976.
15. Robert NJ, Dieras V, Glaspy J, Brufsky AM, Bondarenko I, Lipatov ON, Perez EA, Yardley DA, Chan SY, Zhou X, Phan SC, O'Shaughnessy J. RIBBON-1: randomized, double-blind, placebo-controlled, phase III trial of chemotherapy with or without bevacizumab for first-line treatment of human epidermal growth factor receptor 2-negative, locally recurrent or metastatic breast cancer. J Clin Oncol 2011; 29(10): 1252–1260.
16. Proposal to withdraw approval for the breast cancer indication for Avastin (bevacizumab). US Food and Drug Administration, 2012. Available from: http://www.fda.gov/downloads/NewsEvents/Newsroom/UCM280546.pdf.
17. Mees G, Dierckx R, Vangestel C, Van de Wiele C. Molecular imaging of hypoxia with radiolabelled agents. Eur J Nucl Med Mol Imag 2009; 36(10): 1674–1686.
18. Pauwels EK, Ribeiro MJ, Stoot JH, McCready VR, Bourguignon M, Maziere B. FDG accumulation and tumor biology. Nucl Med Biol 1998; 25(4): 317–322.
19. Busk M, Horsman MR, Jakobsen S, Bussink J, van der Kogel A, Overgaard J. Cellular uptake of PET tracers of glucose metabolism and hypoxia and their linkage. Eur J Nucl Med Mol Imag 2008; 35(12): 2294–2303.
20. Contractor KB, Aboagye EO. Monitoring predominantly cytostatic treatment response with 18F-FDG PET. J Nucl Med 2009; 50(suppl 1): 97S–105S.
21. de Langen AJ, van dBV, Lubberink M, Backes WH, Marcus JT, van TH, Pruim J, Brans B, Leffers P, Dingemans AM, Smit EF, Groen HJ, Hoekstra OS. Monitoring response to antiangiogenic therapy in non-small cell lung cancer using imaging markers derived from PET and dynamic contrast-enhanced MRI. J Nucl Med 2011; 52(1): 48–55.
22. Goshen E, Davidson T, Zwas ST, Aderka D. PET/CT in the evaluation of response to treatment of liver metastases from colorectal cancer with bevacizumab and irinotecan. Technol Cancer Res Treat 2006; 5(1): 37–43.
23. Vriens D, de Geus-Oei LF, Heerschap A, van Laarhoven HW, Oyen WJ. Vascular and metabolic response to bevacizumab-containing regimens in two patients with colorectal liver metastases measured by dynamic contrast-enhanced MRI and dynamic 18F-FDG-PET. Clin Colorectal Cancer 2011; 10(1): E1–E5.
24. Hirashima Y, Yamada Y, Tateishi U, Kato K, Miyake M, Horita Y, Akiyoshi K, Takashima A, Okita N, Takahari D, Nakajima T, Hamaguchi T, Shimada Y, Shirao K. Pharmacokinetic parameters from 3-Tesla DCE-MRI as surrogate biomarkers of antitumor effects of bevacizumab plus FOLFIRI in colorectal cancer with liver metastasis. Int J Cancer 2012; 130(10): 2359–2365.

25. Ungersma SE, Pacheco G, Ho C, Yee SF, Ross J, van BN, Peale FV Jr, Ross S, Carano RA. Vessel imaging with viable tumor analysis for quantification of tumor angiogenesis. Magn ResonMed 2010; 63(6): 1637–1647.
26. Chavhan GB, Babyn PS, Thomas B, Shroff MM, Haacke EM. Principles, techniques, and applications of T_2*-based MR imaging and its special applications. Radiographics 2009; 29(5): 1433–1449.
27. Howe FA, Robinson SP, McIntyre DJ, Stubbs M, Griffiths JR. Issues in flow and oxygenation dependent contrast (FLOOD) imaging of tumours. NMR Biomed 2001; 14(7–8): 497–506.
28. Hittmair K, Gomiscek G, Langenberger K, Recht M, Imhof H, Kramer J. Method for the quantitative assessment of contrast agent uptake in dynamic contrast-enhanced MRI. Magn Reson Med 1994; 31(5): 567–571.
29. Hendriksen EM, Span PN, Schuuring J, Peters JP, Sweep FC, van der Kogel AJ, Bussink J. Angiogenesis, hypoxia and VEGF expression during tumour growth in a human xenograft tumour model. Microvasc Res 2009; 77(2): 96–103.
30. Findlay M, Young H, Cunningham D, Iveson A, Cronin B, Hickish T, Pratt B, Husband J, Flower M, Ott R. Noninvasive monitoring of tumor metabolism using fluorodeoxyglucose and positron emission tomography in colorectal cancer liver metastases: correlation with tumor response to fluorouracil. J Clin Oncol 1996; 14(3): 700–708.
31. Van der Veldt AA, Lubberink M, Bahce I, Walraven M, de Boer MP, Greuter HN, Hendrikse NH, Eriksson J, Windhorst AD, Postmus PE, Verheul HM, Serne EH, Lammertsma AA, Smit EF. Rapid decrease in delivery of chemotherapy to tumors after anti-VEGF therapy: implications for scheduling of anti-angiogenic drugs. Cancer Cell 2012; 21(1): 82–91.
32. Pastuskovas CV, Mundo EE, Williams SP, Nayak TK, Ho J, Ulufatu S, Clark S, Ross S, Cheng E, Parsons-Reponte K, Cain G, Van Hoy M, Majidy N, Bheddah S, dela Cruz Chuh J, Kozak KR, Lewin-Koh N, Nauka P, Bumbaca D, Sliwkowski M, Tibbitts J, Theil FP, Fielder PJ, Khawli LA, Boswell CA. Effects of anti-VEGF on pharmacokinetics, biodistribution, and tumor penetration of trastuzumab in a preclinical breast cancer model. Mol Cancer Ther 2012; 11(3): 752–762.
33. Heskamp S, Boerman OC, Molkenboer-Kuenen JD, Oyen WJ, van der Graaf WT, van Laarhoven HW. Bevacizumab reduces tumor targeting of antiepidermal growth factor and anti-insulin-like growth factor 1 receptor antibodies. Int J Cancer 2013; 133(2): 307–14.
34. Tol J, Koopman M, Cats A, Rodenburg CJ, Creemers GJ, Schrama JG, Erdkamp FL, Vos AH, van Groeningen CJ, Sinnige HA, Richel DJ, Voest EE, Dijkstra JR, Vink-Borger ME, Antonini NF, Mol L, van Krieken JH, Dalesio O, Punt CJ. Chemotherapy, bevacizumab, and cetuximab in metastatic colorectal cancer. New Engl J Med 2009; 360(6): 563–572.
35. Lee ST, Scott AM. Hypoxia positron emission tomography imaging with 18F-fluoromisonidazole. Sem Nucl Med 2007; 37(6): 451–461.
36. Oehler C, O'Donoghue JA, Russell J, Zanzonico P, Lorenzen S, Ling CC, Carlin S. 18F-fluromisonidazole PET imaging as a biomarker for the response to 5,6-dimethylxanthenone-4-acetic acid in colorectal xenograft tumors. J Nucl Med 2011; 52(3): 437–444.
37. Masunaga S, Liu Y, Tanaka H, Sakurai Y, Suzuki M, Kondo N, Maruhashi A, Ono K. Reducing intratumour acute hypoxia through bevacizumab treatment, referring to the response of quiescent tumour cells and metastatic potential. Br J Radiol 2011; 84(1008): 1131–1138.
38. McGee MC, Hamner JB, Williams RF, Rosati SF, Sims TL, Ng CY, Gaber MW, Calabrese C, Wu J, Nathwani AC, Duntsch C, Merchant TE, Davidoff AM. Improved intratumoral oxygenation through vascular normalization increases glioma sensitivity to ionizing radiation. Int J Radiat Oncol Biol Phys 2010; 76(5): 1537–1545.
39. Weisshardt P, Trarbach T, Durig J, Paul A, Reis H, Tilki D, Miroschnik I, Ergun S, Klein D. Tumor vessel stabilization and remodeling by anti-angiogenic therapy with bevacizumab. Histochem Cell Biol 2012; 137 (3): 391–401.
40. Paez-Ribes M, Allen E, Hudock J, Takeda T, Okuyama H, Vinals F, Inoue M, Bergers G, Hanahan D, Casanovas O. Antiangiogenic therapy elicits malignant progression of tumors to increased local invasion and distant metastasis. Cancer Cell 2009; 15(3): 220–231.
41. Rapisarda A, Hollingshead M, Uranchimeg B, Bonomi CA, Borgel SD, Carter JP, Gehrs B, Raffeld M, Kinders RJ, Parchment R, Anver MR, Shoemaker RH, Melillo G. Increased antitumor activity of bevacizumab in combination with hypoxia inducible factor-1 inhibition. Mol Cancer Ther 2009; 8(7): 1867–1877.
42. Ren Y, Fleischmann D, Foygel K, Molvin L, Lutz AM, Koong AC, Jeffrey RB, Tian L, Willmann JK. Antiangiogenic and radiation therapy: early effects on in vivo computed tomography perfusion parameters in human colon cancer xenografts in mice. Invest Radiol 2012; 47(1): 25–32.
43. Airley RE, Loncaster J, Raleigh JA, Harris AL, Davidson SE, Hunter RD, West CM, Stratford IJ. GLUT-1 and CAIX as intrinsic markers of hypoxia in carcinoma of the cervix: relationship to pimonidazole binding. Int J Cancer 2003; 104(1): 85–91.
44. Mehta S, Hughes N, Jubb A, Turley H, Han C, Li S, Taylor N, Padhani A, Adams R, Makris A, Harris A. Early changes in angiogenesis and hypoxia following bevacizumab therapy in primary breast cancer. J Clin Oncol 2012; 30(suppl; abstr 1066).
45. McIntyre A, Patiar S, Wigfield S, Li JL, Ledaki I, Turley H, Leek R, Snell C, Gatter K, Sly WS, Vaughan-Jones RD, Swietach P, Harris AL. Carbonic anhydrase IX promotes tumor growth and necrosis in vivo and inhibition enhances anti-VEGF therapy. Clin Cancer Res 2012; 18(11): 3100–3111.

